



# Dynamic equilibrium of MoSi<sub>2</sub> polymorphs during mechanical milling

Kosuke O. Hara\*, Eiji Yamasue, Hideyuki Okumura, Keiichi N. Ishihara

Graduate School of Energy Science, Kyoto University, Sakyo-ku, Kyoto 606-8501, Japan

## ARTICLE INFO

### Article history:

Received 6 July 2010

Received in revised form 31 January 2011

Accepted 1 February 2011

Available online 31 March 2011

### Keywords:

Mechanical alloying

Intermetallics

Phase transitions

X-ray diffraction

## ABSTRACT

The phase transformation of  $\alpha$ -MoSi<sub>2</sub> into  $\beta$ -MoSi<sub>2</sub> induced by mechanical milling (MM) was studied. Planetary ball milling was performed on an  $\alpha$ -MoSi<sub>2</sub> powder under six different milling conditions. The X-ray diffraction results show that the dynamic equilibrium between  $\alpha$ -MoSi<sub>2</sub> and  $\beta$ -MoSi<sub>2</sub> is reached at low milling intensities, while a single phase of  $\beta$ -MoSi<sub>2</sub> is formed when milled at high milling intensities. The single-phase  $\beta$ -MoSi<sub>2</sub> formation is found to be due to Fe impurity. The mechanism of the phase transformation of MoSi<sub>2</sub> is discussed, and the phase fractions under the dynamic equilibrium are explained by the redistribution of the close-packed layers via synchroshear processes.

© 2011 Elsevier B.V. All rights reserved.

## 1. Introduction

The synthesis of MoSi<sub>2</sub> from an elemental mixture through mechanical alloying (MA) has been extensively studied [1–7]. It is reported that the stable  $\alpha$ -MoSi<sub>2</sub> phase with the C11<sub>b</sub> structure is formed via self-propagating reaction mode when milled at sufficiently high intensity, while low-intensity milling leads to the formation of the metastable  $\beta$ -MoSi<sub>2</sub> phase with the C40 structure together with the  $\alpha$ -MoSi<sub>2</sub> phase [2,4,6]. By further milling, the produced  $\alpha$ -MoSi<sub>2</sub> phase transforms into the  $\beta$ -MoSi<sub>2</sub> phase [5–7]. The relative phase fractions are invariant after long milling time [5]. Such a situation is termed “dynamic equilibrium” [8].

Bokhonov et al. [3] suggested two mechanisms on the phase transformation of MoSi<sub>2</sub>: One ascribes the stabilization of  $\beta$ -MoSi<sub>2</sub> to the increased surface energy of  $\alpha$ -MoSi<sub>2</sub> with reduced particle sizes, while another claims the redistribution of close-packed layers in the  $\alpha$ -MoSi<sub>2</sub> structure, since  $\alpha$ -MoSi<sub>2</sub> and  $\beta$ -MoSi<sub>2</sub> are polytypes. On the other hand, Kang and Yin attributed the formation of  $\beta$ -MoSi<sub>2</sub> to nanocrystallization, based on the estimated crystallite size [6].

The dynamic equilibrium, however, has not been considered in the above proposed mechanisms. Also, there is paucity of the report on the mechanical milling (MM) starting with a single phase MoSi<sub>2</sub>. The aim of this study is thus to investigate in detail the milling-induced phase transformation of MoSi<sub>2</sub>. The transformation mechanism will be discussed from the viewpoint of the redistribution of close-packed layers.

## 2. Experimental

An  $\alpha$ -MoSi<sub>2</sub> powder (Kojundo Chemical Lab., 99.9% grade in purity) was placed in a tool steel vessel (156 ml in volume) with 160 g of bearing steel balls (9.5 mm in diameter) under Ar atmosphere, and then subjected to MM with a planetary ball mill (Fritsch, P5). Six different milling conditions were used by changing the revolution speed ( $\omega$  = 200, 300 and 400 rpm) and the powder weight (4 and 8 g, corresponding to the ball-to-powder weight ratios of 40/1 and 20/1, respectively). The MM conditions will be denoted as “MMxxx-yy”, where “xxx” and “yy” mean revolution speed (rpm) and ball-to-powder weight ratio yy/1, respectively.

The obtained powders were characterized by powder X-ray diffractometry (XRD; RIGAKU RINT-2100 with Cu K $\alpha$  radiation) and energy-dispersive X-ray spectroscopy (EDX; Phoenix EDAX equipment).

The molar fractions of the  $\alpha$  and  $\beta$  phases were determined from the best fit of a simulated XRD pattern to the observed one in the range of  $2\theta$  = 18–40°. The peak profile was expressed by a pseudo-Voigt function. For the 002 and 101 peaks of  $\alpha$ -MoSi<sub>2</sub> ( $2\theta$  = 22.6° and 30.1°, respectively) and the 100, 101 and 102 peaks of  $\beta$ -MoSi<sub>2</sub> ( $2\theta$  = 22.3°, 26.2° and 35.5°, respectively), the integrated intensity was expressed by

$$I_{hkl,n} = C_1 \cdot x_n \cdot \frac{|F_{hkl,n}|^2 m_{hkl,n} L(2\theta)}{V_n^2}, \quad (1)$$

where  $I_{hkl,n}$ ,  $F_{hkl,n}$  and  $m_{hkl,n}$  are the integrated intensity, the crystal structure factor and the multiplicity factor of the  $hkl$  peak of the  $n$  phase ( $n = \alpha$ - or  $\beta$ -MoSi<sub>2</sub>), respectively.  $x_n$  and  $V_n$  are the molar fraction and the unit cell volume of the  $n$  phase, respectively.  $C_1$  is the scaling factor, and  $L(2\theta)$  is the Lorentz-polarization factor. In Eq. (1),  $C_1$  and  $x_n$  are refinable parameters. The proportional relation between the total intensity of a reflected X-ray from a mixture of polymorphs and the molar fraction of the phase corresponding to the reflection [9] was used to derive the equation. For the peak of  $2\theta$  = 39–40°, the integrated intensity was independently refined since it overlaps with another peak of higher angles.

The results from different milling conditions are compared in terms of the total energy given to the unit weight of powder ( $E$ ). It is reported that the power transferred to the powder is proportional to  $\omega^3$ , where  $\omega$  is the revolution speed of a mill [10–12].  $E$  is hence proportional to  $\omega^3 t$ , where  $t$  is the milling time. The value per unit weight of powder is thus expressed as  $E = C_2 \omega^3 t/w$ , where  $C_2$  is a constant and  $w$  is the weight of powder. Since the absolute value is not important,  $E$  was rescaled by setting the  $C_2$  value so that  $E$  is equal to one

\* Corresponding author. Tel.: +81 75 753 5488; fax: +81 75 753 5488.

E-mail address: [hara@namihei.mtl.kyoto-u.ac.jp](mailto:hara@namihei.mtl.kyoto-u.ac.jp) (K.O. Hara).

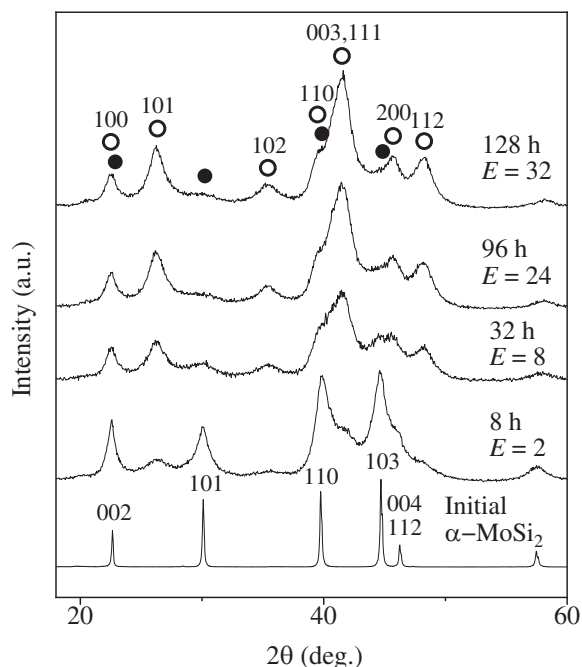


**Fig. 1.** The XRD patterns of the  $\text{MoSi}_2$  powders milled under the MM300-20 condition, and of the initial  $\alpha\text{-MoSi}_2$  powder ((●)  $\alpha\text{-MoSi}_2$ , (○)  $\beta\text{-MoSi}_2$ ).

for the smallest total-energy condition employed, i.e.  $\omega=300$  rpm,  $w=8$  g and  $t=4$  h.

### 3. Results

**Fig. 1** shows the XRD patterns of the  $\text{MoSi}_2$  powders (MM300-20). The pattern of the initial  $\alpha\text{-MoSi}_2$  powder is also displayed. The peaks of  $\beta\text{-MoSi}_2$  become gradually higher on milling. The XRD pattern for 128 h-milled powder includes both  $\alpha\text{-MoSi}_2$  and  $\beta\text{-MoSi}_2$  peaks, which is almost the same as that for 96 h-milled one, indicating that the system reaches a dynamic equilibrium state. When other conditions (MM400-20, MM200-40 and MM200-20) are used, the dynamic equilibrium between  $\alpha$  and  $\beta\text{-MoSi}_2$  is also reached.

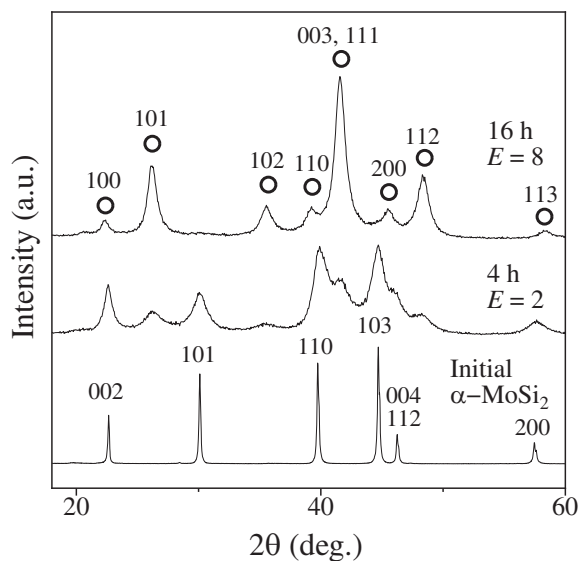


**Fig. 2.** The XRD patterns of the  $\text{MoSi}_2$  powders milled under the MM300-40 condition, and of the initial  $\alpha\text{-MoSi}_2$  powder ((○)  $\beta\text{-MoSi}_2$ ).

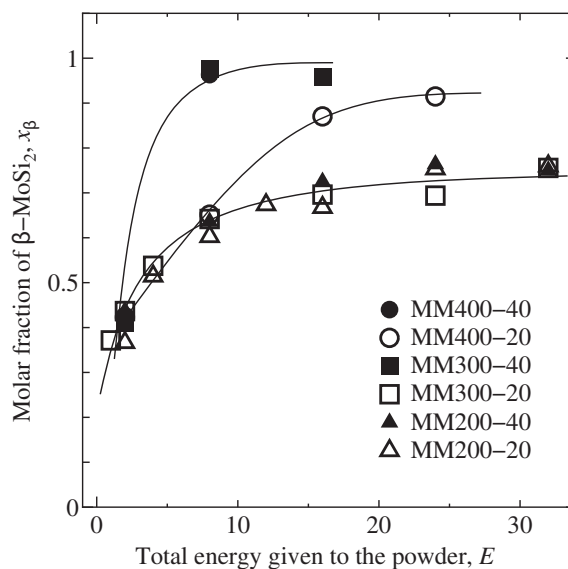


**Fig. 3.** The molar fraction of  $\beta\text{-MoSi}_2$  ( $x_\beta$ ) in the milled powders as a function of the total energy given to the powder ( $E$ ). The lines are only a guide for the eyes.

In contrast, a single phase of  $\beta\text{-MoSi}_2$  is obtained when milled under other conditions (MM400-40 and MM300-40). **Fig. 2** shows the XRD patterns for the MM300-40 condition. The peaks of  $\beta\text{-MoSi}_2$  are detected in the 4 h-milled powder, and after 16 h of MM only  $\beta\text{-MoSi}_2$  peaks are seen. The  $\text{MoSi}_2$  powder (MM400-40) also shows the XRD pattern of a single phase of  $\beta\text{-MoSi}_2$  after 6.75 h of MM.

**Fig. 3** shows the molar fraction of  $\beta\text{-MoSi}_2$  ( $x_\beta$ ) as a function of the total energy given to the powder ( $E$ ). The  $x_\beta$  value increases with increasing  $E$ , and becomes a steady state after prolonged milling. The powders of  $E > 15$  and those of a single phase of  $\beta\text{-MoSi}_2$  will be regarded as in the “steady state” hereafter. It is seen from **Fig. 3** that the steady-state  $x_\beta$  values are larger under the higher milling intensities (power input per sample weight).

Strong ball impacts may lead to much ball debris. According to the EDX results, the powders produced with the high milling intensities contain Fe and Cr impurities, the amount of Cr being less than 5 at% of Fe. Thus, the formation of  $\beta\text{-MoSi}_2$  is possibly due to Fe contamination. To examine the effects of the Fe contamination on the transformation, an Fe powder (Kojundo Chemical Lab., 99.9% up, 150  $\mu\text{m}$  pass) was deliberately added to the initial  $\alpha\text{-MoSi}_2$  powder, and subjected to MM under the MM300-20 condition. **Fig. 4** shows the XRD pattern of the milled  $\text{MoSi}_2\text{-Fe}$  powder mixture. The milled  $\text{MoSi}_2\text{-Fe}$  mixture contains 7.4 at% of Fe after 96 h-milling,

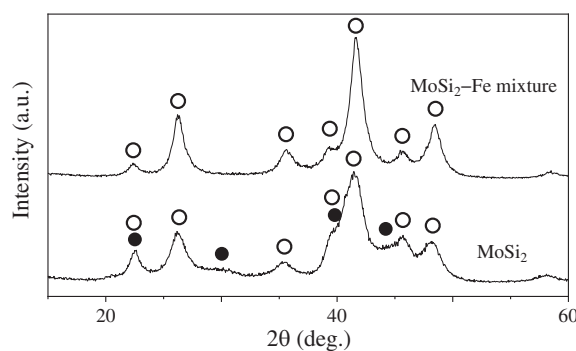


**Fig. 4.** The XRD patterns of the  $\text{MoSi}_2\text{-Fe}$  powder mixture milled under the MM300-20 condition for 96 h, along with the  $\text{MoSi}_2$  powder milled in the same way ((●)  $\alpha\text{-MoSi}_2$ , (○)  $\beta\text{-MoSi}_2$ ).

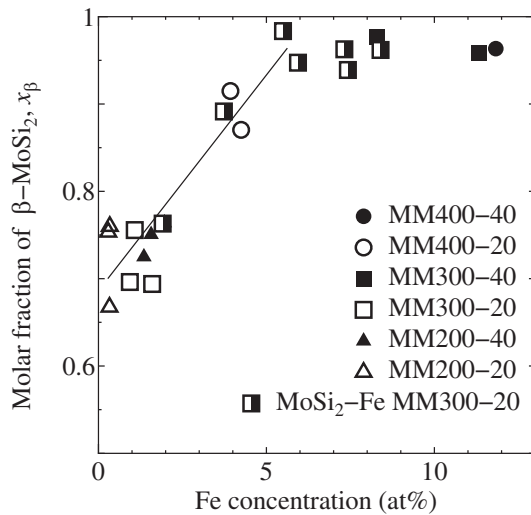


Fig. 5. The molar fraction of  $\beta$ - $\text{MoSi}_2$  ( $x_\beta$ ) as a function of Fe concentration for the steady-state powders.

and shows single-phase  $\beta$ - $\text{MoSi}_2$  peaks, while the  $\text{MoSi}_2$  powder milled under the same condition contains 1.6 at% of Fe, and shows both  $\alpha$ - $\text{MoSi}_2$  and  $\beta$ - $\text{MoSi}_2$  peaks. It suggests that Fe impurity promotes the formation of  $\beta$ - $\text{MoSi}_2$ .

The steady-state  $x_\beta$  value is plotted as a function of Fe amount in Fig. 5. A positive correlation between  $x_\beta$  and Fe amount is seen. Since the powders with similar Fe amounts show similar  $x_\beta$  values regardless of the different milling conditions, the milling intensity does not seem to have significant effects on the  $x_\beta$  value at the dynamic equilibrium. Furthermore, the  $x_\beta$  value at no impurity is estimated to be  $x_\beta = 0.7$ , which is close to the value reported by Heron and Schaffer for the MA starting with an elemental mixture (0.683) [5].

#### 4. Discussion

Both the  $\text{C11}_b$  ( $\alpha$ - $\text{MoSi}_2$ ) and  $\text{C40}$  structures ( $\beta$ - $\text{MoSi}_2$ ) commonly possess close-packed  $\text{MoSi}_2$  layers, and differ from each other only in the stacking sequence of these layers: the AB and ABC stacking for the  $\text{C11}_b$  and  $\text{C40}$  structures, respectively. Fig. 6 shows the atomic arrangement of the B close-packed layer put on the A layer. C and D stacking positions also lead to the same nearest-neighbor environment of atoms.

Bokhonov et al. suggested that the transformation into  $\beta$ - $\text{MoSi}_2$  proceeds by plastic deformation owing to the redistribution of close-packed layers in the  $\alpha$ - $\text{MoSi}_2$  structure [3]. They did not report, however, how the close-packed layers move during deformation. Inui et al. observed the synchroshear mechanism in the plastic deformation of  $\text{CrSi}_2$  and  $\text{Mo}(\text{Si, Al})_2$  both with the  $\text{C40}$  structure, and also proposed that the synchroshear mechanism plays a role in the transformations between  $\text{C11}_b$  and  $\text{C40}$  phases [13,14]. That is, if a C layer above a B layer and all successively upper layers are displaced by  $\pm \frac{1}{6}[1\bar{1}2\bar{0}]$  and at the same time, an A layer above the C layer and all successively upper layers are displaced by  $\pm \frac{1}{6}[\bar{1}2\bar{1}0]$ , the stacking sequence of the BCA unit is transformed into the AB-type sequence. The  $\text{C40}$  structure is transformed into the  $\text{C11}_b$  structure if such synchronous displacements are continued unit by unit. The  $\text{C11}_b$  structure is also transformed reversely into the  $\text{C40}$  structure through a similar shear mechanism.

Such continuous synchroshear displacement may be energetically favored during severe deformation. Basal slips are operative both in the  $\text{C11}_b$  and  $\text{C40}$  silicides [15–17]. The basal slip vectors usually dissociate as  $\frac{1}{2}(111) \rightarrow \frac{1}{4}(111) + \text{SISF} + \frac{1}{4}(111)$  in the

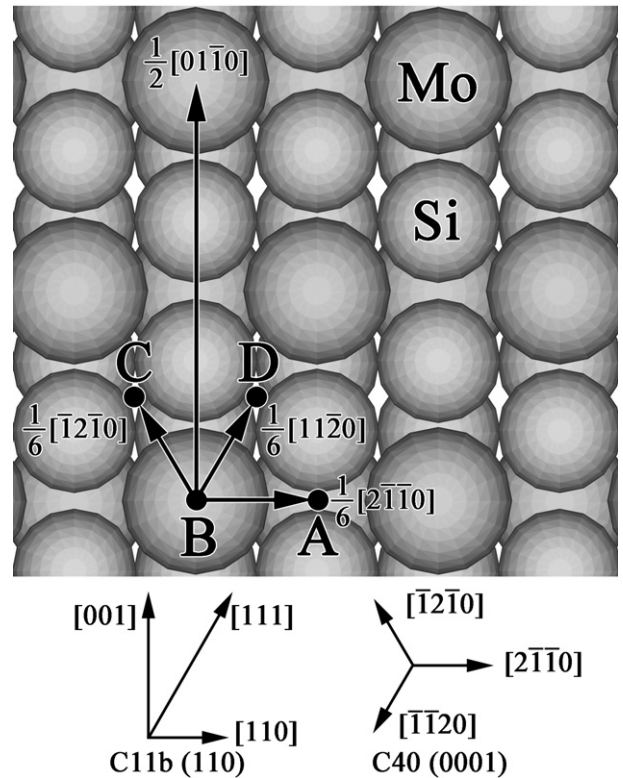


Fig. 6. Atomic arrangement on (110) in the  $\text{C11}_b$  structure and (0001) planes in the  $\text{C40}$  structure. The stacking positions of A–D and crystallographic directions with respect to both  $\text{C11}_b$  and  $\text{C40}$  structures are indicated. Large and small circles correspond to the Mo and Si atoms, respectively.

$\text{C11}_b$  structure, and  $\frac{1}{3}(11\bar{1}20) \rightarrow \frac{1}{6}(11\bar{1}20) + \text{SF} + \frac{1}{6}(11\bar{1}20)$  in the  $\text{C40}$  structure, where a superlattice intrinsic stacking fault (SISF) or a stacking fault (SF) is produced. These faults raise the system energy. When the more severe the deformation is, the higher the system energy becomes. The synchroshears, on the other hand, enable deformation without producing stacking faults but with a phase transformation.

Considering the  $[01\bar{1}0]$  direction force applied to the close-packed layers of the  $\alpha$ - $\text{MoSi}_2$  phase, phase transformation into the  $\beta$ - $\text{MoSi}_2$  phase may occur by the motion of the synchroshears consisting of  $\frac{1}{6}[\bar{1}2\bar{1}0]$  and  $\frac{1}{6}[11\bar{1}20]$  partials. Two modes are possible depending on the order of  $\frac{1}{6}[\bar{1}2\bar{1}0]$  and  $\frac{1}{6}[11\bar{1}20]$  to appear. It should be noted that the  $\beta$ - $\text{MoSi}_2$  crystals produced by the different sequence of synchroshears belong to different space groups ( $P6_222$  and  $P6_422$ ), which are enantiomorphically related. On the other hand, the  $\beta$ - $\text{MoSi}_2$  phase transforms into the  $\alpha$ - $\text{MoSi}_2$  phase by one of the two modes, while the other mode is unrealistic because of a geometrical reason: if a C layer above a B layer is displaced by  $\pm \frac{1}{6}[\bar{1}2\bar{1}0]$ , two B layers appear successively, where the system energy increases.

According to the above consideration, the rate constant of the  $\alpha \rightarrow \beta$  transformation ( $k_1$ ) is twice larger than that for the  $\beta \rightarrow \alpha$  transformation ( $k_2$ ). Assuming the first-order rate law for simplicity,  $v_{\alpha \rightarrow \beta} = k_1(1 - x_\beta)$ ,  $v_{\beta \rightarrow \alpha} = k_2 x_\beta$ ,  $k_1 = 2k_2$ , where  $v_{\alpha \rightarrow \beta}$  and  $v_{\beta \rightarrow \alpha}$  are the transformation rates of the  $\alpha \rightarrow \beta$  and  $\beta \rightarrow \alpha$  transformations, respectively. Since  $v_{\alpha \rightarrow \beta}$  is equal to  $v_{\beta \rightarrow \alpha}$  under the dynamic equilibrium condition, the predicted  $x_\beta$  value is  $2/3$ , which is close to the obtained value of 0.7. The dynamic equilibrium of  $\text{MoSi}_2$  polymorphs is, therefore, quantitatively explained.

Since the reason why Fe impurity promotes the formation of  $\beta$ - $\text{MoSi}_2$  still remains to be solved, more work is needed on this point. For example, the chemical reaction between  $\text{MoSi}_2$  and Fe

should be investigated. The results will be published in a separate paper.

## 5. Conclusion

Mechanical milling of an  $\alpha$ -MoSi<sub>2</sub> powder was studied. The  $\alpha$ -MoSi<sub>2</sub> phase transforms into the metastable  $\beta$ -MoSi<sub>2</sub> phase during MM, and the dynamic equilibrium between  $\alpha$ -MoSi<sub>2</sub> and  $\beta$ -MoSi<sub>2</sub> is reached. Fe impurity promotes the formation of  $\beta$ -MoSi<sub>2</sub>, while the milling intensity does not seem to have significant effects on the phase fractions at the dynamic equilibrium. The molar fractions under the dynamic equilibrium are explained by the synchroshear mechanism.

## Acknowledgement

This work is partly supported by the Kyoto University Global COE Program, “Energy Science in the Age of Global Warming”.

## References

- [1] R. Schwarz, S. Srinivasan, J. Petrovic, C. Maggiore, *Mater. Sci. Eng. A* 155 (1992) 75–83.
- [2] S. Patankar, S. Xiao, J. Lewandowski, A. Heuer, *J. Mater. Res.* 8 (1993) 1311–1316.
- [3] B. Bokhonov, I. Konstanchuk, V. Boldyrev, *J. Alloys Compd.* 218 (1995) 190–196.
- [4] L. Liu, K. Cui, *J. Mater. Process. Technol.* 138 (2003) 394–398.
- [5] A. Heron, G. Schaffer, *Mater. Sci. Eng. A* 352 (2003) 105–111.
- [6] P. Kang, Z. Yin, *Nanotechnology* 15 (2004) 851–855.
- [7] C. Lee, *J. Ceram. Process. Res.* 9 (2008) 321–324.
- [8] E. Gaffet, *Mater. Sci. Eng. A* 119 (1989) 185–197.
- [9] L. Alexander, H. Klug, *Anal. Chem.* 20 (1948) 886–889.
- [10] M. Magini, A. Iasonna, *Mater. Trans., JIM* 36 (1995) 123–133.
- [11] M. Magini, A. Iasonna, F. Padella, *Scripta Mater.* 34 (1996) 13–19.
- [12] J. Ipus, J. Blázquez, V. Franco, M. Millán, A. Conde, D. Oleszak, T. Kulik, *Intermetallics* 16 (2008) 470–478.
- [13] H. Inui, M. Moriwaki, S. Ando, M. Yamaguchi, *Mater. Sci. Eng. A* 239–240 (1997) 63–68.
- [14] H. Inui, M. Moriwaki, K. Ito, M. Yamaguchi, *Philos. Mag. A* 77 (1998) 375–394.
- [15] K. Ito, H. Inui, Y. Shirai, M. Yamaguchi, *Philos. Mag. A* 72 (1995) 1075–1097.
- [16] K. Ito, T. Yano, T. Nakamoto, H. Inui, M. Yamaguchi, *Acta Mater.* 47 (1999) 937–949.
- [17] H. Inui, M. Yamaguchi, *Intermetallics* 9 (2001) 857–862.